JACS Au
AN OPEN ACCESS JOURNAL OF THE AMERICAN CHEMICAL SOCIETY

pubs.acs.org/jacsau

Article

# Harvesting High-Quality White-Light Emitting and Remarkable Emission Enhancement in One-Dimensional Halide Perovskites Upon Compression

Yuanyuan Fang, Tianyin Shao, Long Zhang, Laizhi Sui, Guorong Wu, Kaijun Yuan, Kai Wang,* and Bo Zou*

Cite This: *JACS Au* 2021, 1, 459–466

Read Online

ACCESS | Metrics & More | Article Recommendations | Supporting Information

**ABSTRACT:** The pressure induced emission (PIE) behavior of halide perovskites has attracted extensive interest due to its potential application in pressure sensors and trademark security. However, the PIE phenomenon of white-light-emitting hybrid perovskites (WHPs) is rare, and that at pressures above 10.0 GPa has never been reported. Here, we effectively adjusted the perovskite to emit high-quality "cold" or "warm" white light and successfully realized pressure-induced emission (PIE) upon even higher pressure up to 35.1 GPa in one-dimensional halide perovskite $C_4N_2H_{14}PbCl_4$. We reveal that the degree of structural distortion and the rearrangement of the multiple self-trapped states position are consistent with the intriguing photoluminescence variation, which is further supported by *in situ* high-pressure synchrotron X-ray diffraction experiments and time-resolved photoluminescence decay dynamics data. The underlying relationship between octahedron behavior and emission plays a key role to obtain high-quality white emission perovskites. We anticipate that this work enhances our understanding of structure-dependent self-trapped exciton (STE) emission characteristics and stimulates the design of high-performance WHPs for next generation white LED lighting devices.

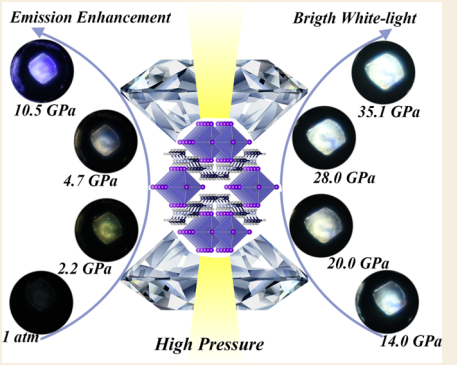


**KEYWORDS:** *pressure-induced emission, one-dimensional perovskite, structural distortion, white-light emitting, self-trapped excitons*

## INTRODUCTION

The low-dimensional halide perovskites (LDHPs) as the derivatives of the traditional $ABX_3$ perovskite structure have shown great potential in the optoelectronic field due to their exceptional stability and excellent optical properties.[1−6] Recently, the ever-growing interest in LDHPs has made them a promising class of semiconductor materials for next-generation solid-state lighting applications.[7−10] However, the development of white perovskite light-emitting diodes (PeLEDs) is limited by the difficulty of obtaining high-quality white perovskite light-emitting layers, which makes their development far behind that of their green and red analogues.[11−16] The one-dimensional (1D) metal halide perovskite $C_4N_2H_{14}PbCl_4$ crystal is identified as the core−shell quantum wire structure which is composed of double edge-sharing octahedral $PbCl_6^{4-}$ chains coated with organic $C_4N_2H_{14}^{2+}$ cations. This distinct 1D quantum-well configuration is prone to multiple self-trapped exciton (STE) states triggering the broadband emission.[17] Therefore, this structural feature makes it an attractive material for light emission devices. However, with the limited degree of distortion in the structure, it approaches excellent enough white emission properties to fabricate high-performance optoelectronic devices. Consequently, finding an effective strategy to modulate the luminescence of $C_4N_2H_{14}PbCl_4$ perovskites would be quite beneficial for their practical applications.

As a controllable and predictable way, pressure is highly instructive for modulating the crystal structures and optical properties of perovskites without changing the composition therein.[18−24] Recently, scientists began to shift the focus from high-pressure 3D perovskites research to LDHPs.[25−29] Notably, the pressure-induced phase transition and band gap structure tuning on LDHPs render the pressure a feasible strategy to optimize its properties.[30−32] For example, the series of LDHPs $[C_nH_{2n+1}NH_3]_2PbI_4$ ($n$ = 4, 8, 12) were confirmed to have longer alkylamine cations that lead to less ease of phase transition upon compression;[33] $(PEA)PbI_4$ was observed to have a direct−indirect band gap transition at around 5.8 GPa,[34] and $BA_2PbBr_4$ was found to have a pressure-induced photoluminescence enhancement below 1.0 GPa.[35] However, current

Received: January 22, 2021
Published: March 2, 2021

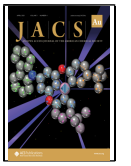

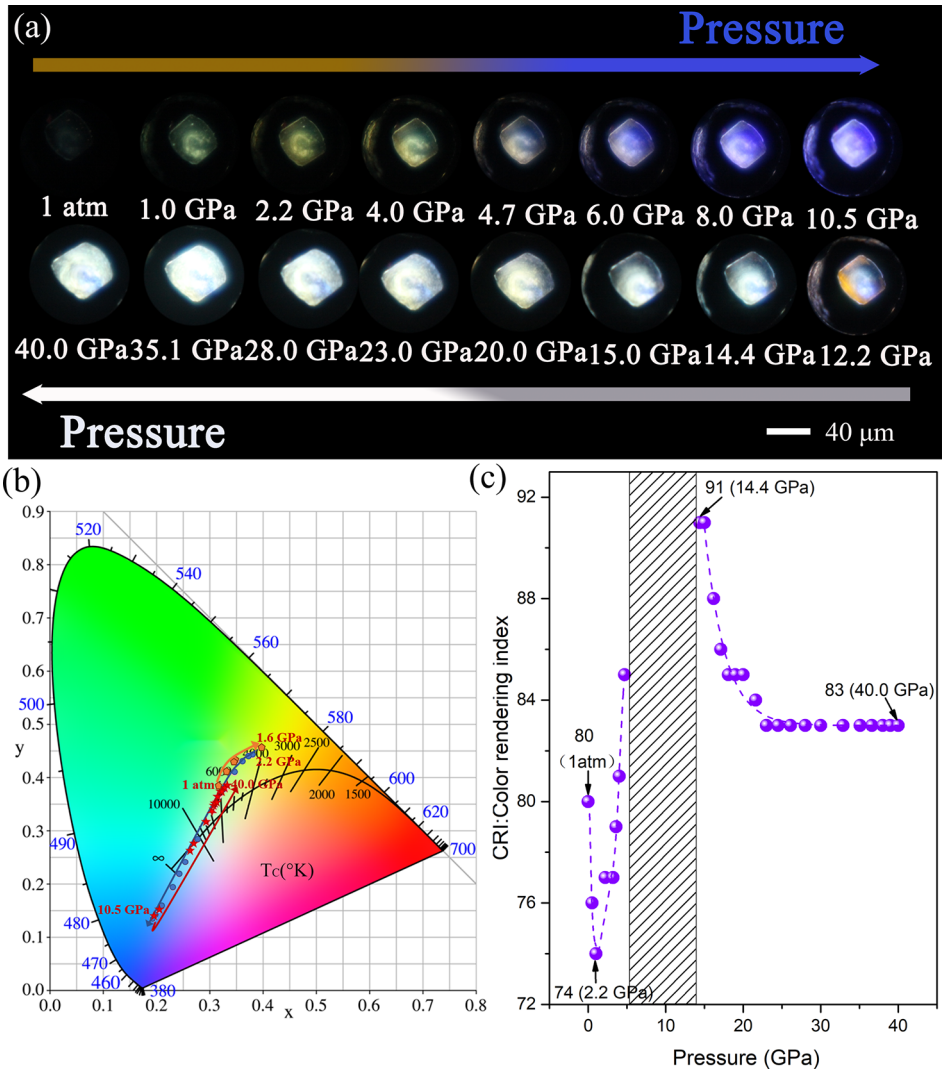


**Figure 1.** (a) PL photographs of $C_4N_2H_{14}PbCl_4$ crystal upon compression up to 40.0 GPa. (b) Chromaticity coordinates of the emissions as a function of pressure. The pressure range from 1 atm to 1.6 GPa is represented by the orange pentagon dots, while the range of 2.2−10.5 GPa is represented by the blue round dots, and the last range of 10.5−40.0 GPa is represented by the red pentacle dots. (c) Color rendering index (CRI) of the $C_4N_2H_{14}PbCl_4$ crystal emissions upon compression; the shadow region is because the correlated color temperatures (CCT) saturation and the CRI of the sample cannot be calculated.

high-pressure studies on LDPHs focus on the low-pressure region to obtain novel optical properties, and these materials are plagued by emission quenched upon higher pressure, which mostly limits their potential applications in ultrahigh-pressure sensors devices.[36−38] Moreover, the pressure responses of white-light-emitting hybrid perovskites (WHPs) remain to be explored. Therefore, the 1D white emission of $C_4N_2H_{14}PbCl_4$ with a soft lattice makes us expect some totally different photophysical properties upon compression.[17]

In this work, we report on the optical properties and crystal structures of $C_4N_2H_{14}PbCl_4$ up to 40.0 GPa. Interestingly, the emission chromaticity of the initial broadband white emissive $C_4N_2H_{14}PbCl_4$ can be continuously and widely adjusted upon compression. More intriguing is that the $C_4N_2H_{14}PbCl_4$ crystal exhibited the periodical pressure-induced emission (PIE) phenomenon until 35.1 GPa, which has never been reported in previous PIE systems. This phenomenon not only breaks the traditional thinking that the pressure-induced PL quenching[31] and the PIE effect only exist in the low-pressure region,[29] but also corrects the misconception that the decrease of crystallinity of perovskite materials will lead to the destruction of optical properties,[36] thus further enriching the concept and scope of the PIE phenomenon. Moreover, the excellent properties of materials under ultrahigh pressure are required in aerospace application field and geological engineering. Our results provide a scientific basis for the potential use of such materials in these extreme conditions. Analysis of combined *in situ* high-pressure synchrotron X-ray diffraction (XRD) and Raman spectroscopy data indicates that apparently structural distortions of both inter- and intraoctahedrons are accompanied by variation of the Pb−Cl−Pb bond. The octahedra distortion degree increase was believed to cause stronger electron−phonon coupling strength and change the multiple STEs state position, corresponding to the unprecedented emission changes of $C_4N_2H_{14}PbCl_4$. Our results could serve as important basics to guide the synthesis of high-quality white perovskite for application in WLEDs.


https://dx.doi.org/10.1021/jacsau.1c00024
JACS Au 2021, 1, 459−466

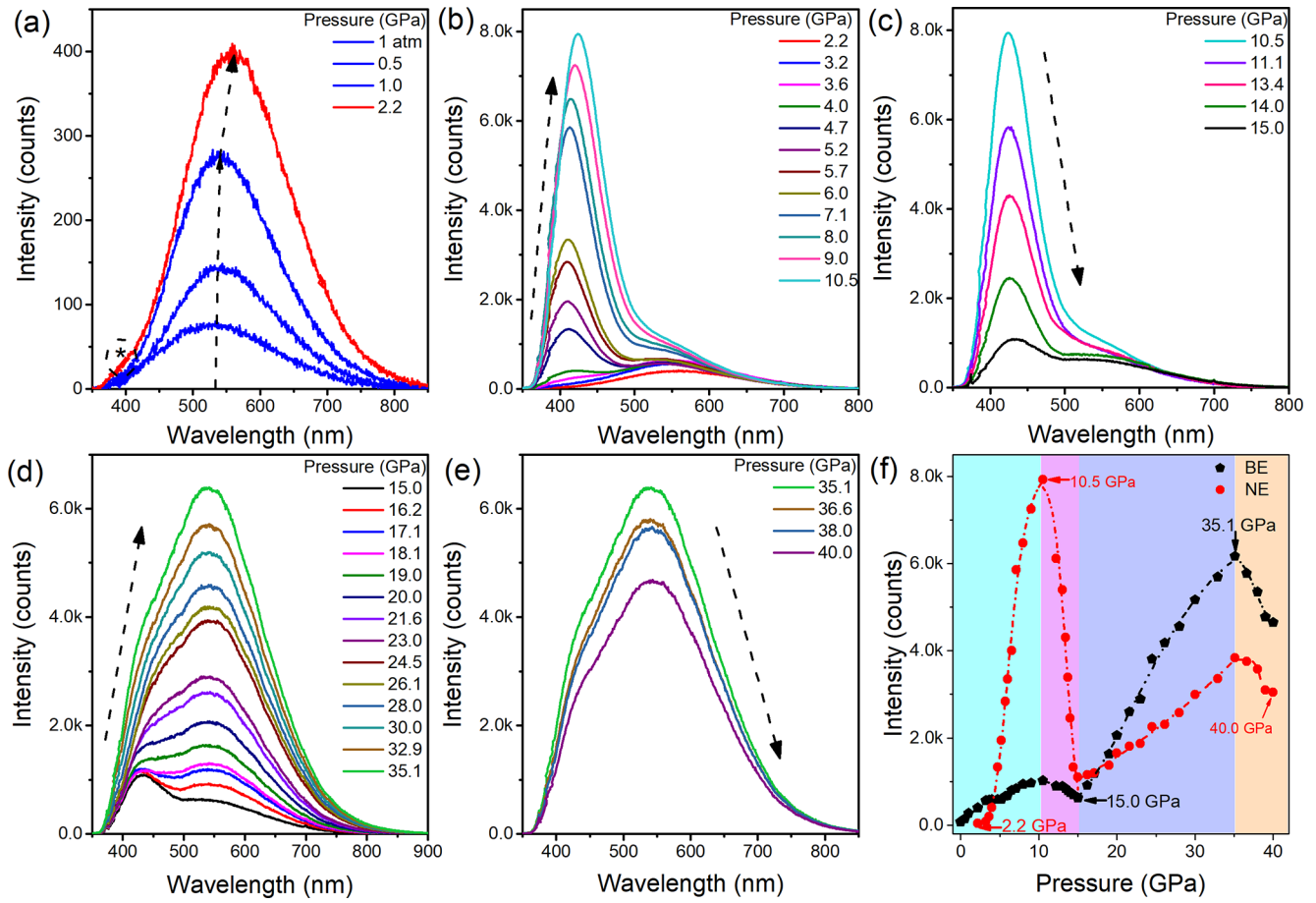


**Figure 2.** (a–e) PL spectra of $C_4N_2H_{14}PbCl_4$ crystal upon compression up to 40.0 GPa. The black arrows represent the changes of the PL intensity. (f) Evolution of the broadband emission (BE) and new emission (NE) peak maximum intensity as a function of pressure up to 40.0 GPa. The BE emission intensity is denoted as black pentagon dots, while the NE emission intensity is denoted as red round dots.

## EXPERIMENTAL DETAILS

### High Pressure

A diamond anvil cell (DAC) with 400 $\mu$m diameter culets was used to reach high pressure conditions. A T301 stainless steel gasket with a 125 $\mu$m hole and 40 $\mu$m thickness served as the sample chamber. The sample was loaded into the sample chamber along with a ruby ball to determine pressure according to the ruby fluorescence technique. In high pressure optical absorption, PL, and XRD experiments, we used silicone oil as a pressure-transmitting medium.

### *In Situ* High-Pressure Optical Measurements

The *in situ* high-pressure PL measurements were carried out using the 355 nm line of a UV DPSS laser. *In situ* high-pressure UV–vis absorption measurements were performed by using a deuterium-halogen light source. The fiber spectrometer used is an Ocean Optics QE65000 spectrometer. The PL micrographs of the samples upon compression were taken with a camera (CanonEos 5D mark II) installed on a microscope (Ecilipse TI-U, Nikon). *In situ* high-pressure Raman spectra were collected by uisng a Raman spectrometer (iHR 550, Symphony II, Horiba Jobin Yvon) with a 785 nm and 10 mW excitation laser.

## RESULTS AND DISCUSSION

The optical micrographs in Figure 1a clearly reveal that the emission peak maintain distinct changes throughout the compression process. Remarkably, the emission of the $C_4N_2H_{14}PbCl_4$ crystal is very bright even at 35.1 GPa. The correlated color temperature (CCT) and color-rendering index (CRI) are two important parameters for white emissive materials. The CCT implies the color of white itself actually changes with a change in its color temperature; it used to further define the color of white emission. CRI reflects the color rendering ability of a light source to objects, and CRI over 80 is the better choice for commercial lighting.[11] Therefore, we record the Comission Internationale de l'Eclairage (CIE) chromaticity coordinate of the crystal emissions upon continuous compression (Figure 1b). At ambient conditions, the emission has a CIE coordinate of (0.32, 0.39), whose CCT is 6058 K, the alleged "cold" white light for LED lighting fixtures. The broadband emission has a CRI of 80, which needs to be improved for practical applications. When the pressure is increased to 1.6 GPa, the $C_4N_2H_{14}PbCl_4$ crystal shifts from "cold" white emission to "warm" white emission with a CCT of 4398 K (Figure S1). After that, the emission color transfers to the cold-white emission direction until it reaches the bright bluish-white emission with over $100 \times 10^3$ K CCT at 10.5 GPa. Upon further compression, the emission color transfers back to the "warm" white emission with 5544 K CCT at 40.0 GPa. Accompanied by the CCT changes, the CRI was also well modulated (Figure 1c). Despite the decrease from 1 atm to 2.2 GPa, the CRI of the $C_4N_2H_{14}PbCl_4$ crystal is obviously enhanced upon further compression until it yields excellent high CRI values of 91 at 14.4 GPa. After that, the CRI decreased with increasing pressure to 20.0 GPa. Then, it became stable with CRI values of 83 until 40.0 GPa, which is higher than that in its ambient condition. Therefore, the high-pressure could be


https://dx.doi.org/10.1021/jacsau.1c00024
JACS Au 2021, 1, 459–466

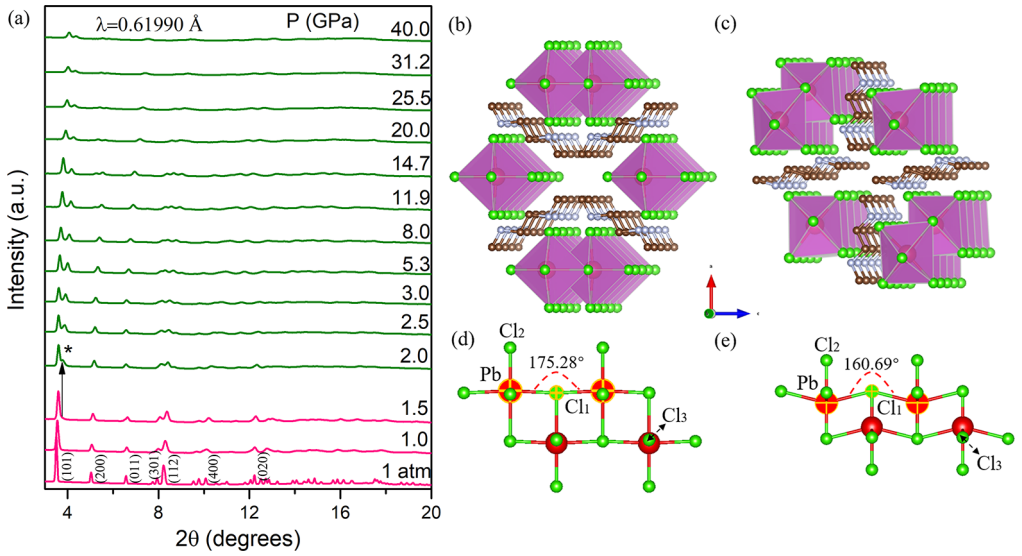


**Figure 3.** (a) Representative XRD patterns of $C_4N_2H_{14}PbCl_4$ at selected pressures up to 40.0 GPa. (b, c) Crystal structure of $C_4N_2H_{14}PbCl_4$ before and after phase transition. (d, e) Schematic illustrations of the Pb−Cl−Pb bond angle within the inorganic layer framework before and after the phase transition.

used as a powerful means to achieve adjustable large-scale emission chromaticity.

Figure 2 shows PL spectra of $C_4N_2H_{14}PbCl_4$ crystal ranging from 0.0 to 40.0 GPa recorded with an excitation wavelength at 355 nm. Under ambient pressure, $C_4N_2H_{14}PbCl_4$ has a quite low brightness broadband white emission with a maximum emission peak at 537 nm and a full width at half-maximum (fwhm) of 207.9 nm, whose Stokes shift up to 207.1 nm (Figure 2a and S2a). This broadband emission is demonstrated to be originated from multiple self-trapped excitons (STEs) emission.[17] Upon compression to 2.2 GPa, the intensity of the original broadband emission (BE) experienced a slight increase which is ascribed to the slight convergence between the inorganic octahedron and organic cations under mild compression.[39] Surprisingly, a new emission (NE) appears with a shorter emission wavelength of 405 nm (~80 nm Stokes shifts Figure S2b), indicating possible structural variations. Under 355 nm excitation, the intensity of both the NE emission and the BE emission show a linear dependence on the excitation power density up to 4 mW/cm$^2$ (Figure S3), suggesting that both emissions originated from STEs.[17] After that, the intensity of the NE peak experiences an obviously continuous increase accompanied by the BE intensity showing a slight increase until 10.5 GPa (Figure 2b and f) which is usually ascribed to the lattice contraction.[40] Meanwhile, the NE emission undergoes a continuous red-shift upon compression from 2.1 to 10.5 GPa. This phenomenon maybe governed by the intermolecular interaction of the inorganic octahedron, which is greatly affected the self-trapped states position. This situation is very similar to the negative ion repulsion of ice and water upon compression.[41−43] Then, both the BE intensity and NE intensity showed a decrease up to 15.0 GPa (Figure 2c). Intriguingly, the intensity of the NE and BE both re-emerged with a distinctly persistent enhancement until 35.1 GPa (Figure 2d). To date, the phenomenon of the emission intensity increase above 10.0 GPa has never been reported in previous PIE systems; this is the first report of bright broadband white-light emission in LDHPs at 35.1 GPa. Then, the following pressure made both emission peaks start to decrease again until 40.0 GPa (Figure 2e), and the PL intensity is already very weak when the pressure is 60.0 GPa (Figure S4), which could be due to the severe structural deformation caused by deviatoric stress.[36] After decompression, the PL spectrum is slightly weaker than the initial state and returns to the original position (Figure S5). These abundant changes can be reproduced in our repeated experiments.

Moreover, high-pressure absorption experiments were performed to trace the band gap modulation (Figure S6a). At ambient conditions, the crystal $C_4N_2H_{14}PbCl_4$ shows an absorption edge located at about 330.9 nm.[17] The band gap ($E_b$) of $C_4N_2H_{14}PbCl_4$ decreases slightly by 0.05 eV when the compression is 1.6 GPa, indicating the feasible organic-to-inorganic approach in the low pressure range.[44] After that, the band gap suddenly increases to 3.83 eV at 2.1 GPa, which coincides with the appearance of the new PL peak. And the color of the sample does not change obviously before and after phase transformation. With further compression, the $E_b$ is slightly decreased from 2.2 to 13.0 GPa, then it experiences a faster rate decrease until 40.0 GPa. This decrease is caused by considerable lattice shrinkage and structural distortion upon enough compression (Figure S6b).[32]

An *in situ* high-pressure angle-dispersive X-ray diffraction (ADXRD) experiment up to 40.0 GPa was performed to understand the relationship between optical response and structural variations of $C_4N_2H_{14}PbCl_4$ (Figure 3a). Upon compression, all the diffraction peaks of original phase shifted to higher angles due to a decrease in the volume of unit cell. At 2.0 GPa, the intensity of the first diffraction peak at ~3.5° corresponding to the Bragg (101) reflection decreased greatly, a new diffraction peak at ~3.8° corresponding to the Bragg (001) reflection emerged, and the diffraction peaks underwent an apparent redistribution of intensities in the 2$\theta$ range of 7−9°, indicating that the sample structure transformed into a new phase (phase II). As the pressure increased further, all the Bragg diffraction peaks shifted to the higher angles without the emergence of new peaks. Especially, from 14.4 to 40.0 GPa, although the intensity of some original reflections decreased and a few bands were broadened, indicating that significant structural distortion occurs, all the peaks did not disappeared, suggesting a long-range order in the crystal structure which may be due to the high electronegativity matching between $Cl^-$ and


https://dx.doi.org/10.1021/jacsau.1c00024
JACS Au 2021, 1, 459−466

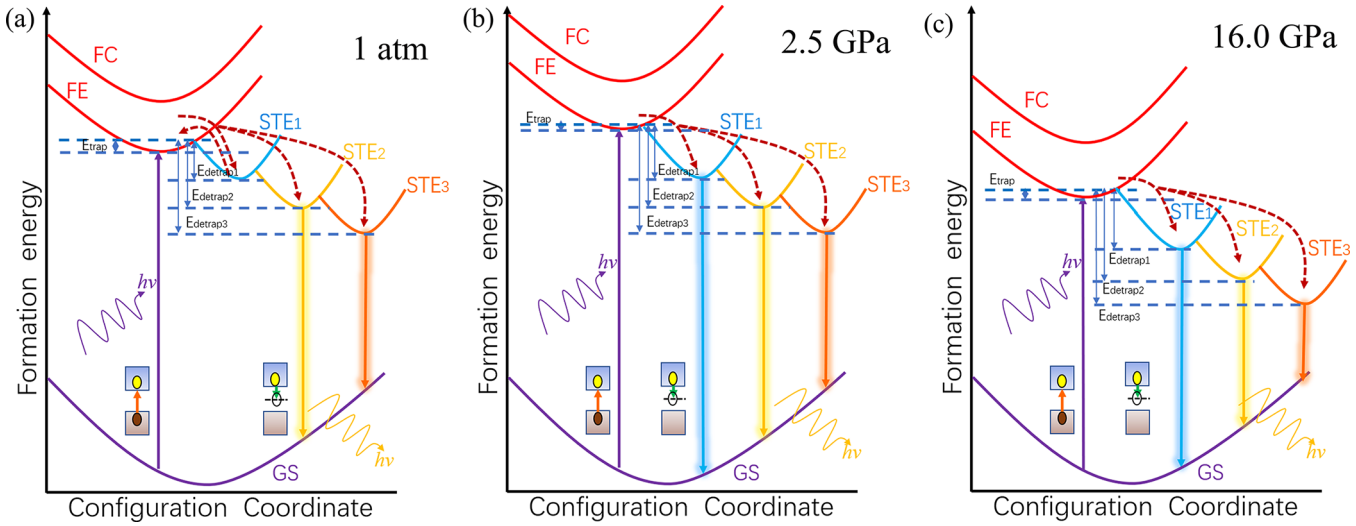


**Figure 4.** Illustrations of PIE mechanism associated with exciton self-trapping (a) at ambient conditions, (b) upon compression at 2.5 GPa, and (c) upon high pressure at 16.0 GPa. Ground state (GS), free exciton state (FE), free-carrier state (FC), and self-trapped exciton state ($STE_1$, $STE_2$, $STE_3$). $E_{trap}$ = activation energy for self-trapping; $E_{detrap}$ = activation energy for detrapping.

$Pb^{2+}$ ions. Different from other perovskites, the beginning of amorphization is always observed around 20.0 GPa.[18,45−47] Therefore, 1D $C_4N_2H_{14}PbCl_4$ crystals can be expected to have some optical properties completely different from those of its 1D analogues in a higher-pressure range.[36,48]

Rietveld refinement results show that the ambient structure of $C_4N_2H_{14}PbCl_4$ is the orthorhombic space group *Imma* with lattice parameters $a$ = 14.11(2), $b$ = 5.82(3), and $c$ = 14.55(2) (Figure S7a and Table S1).[17] Then, the crystal structure transforms into triclinic space group $P-1$ with lattice parameters $a$ = 9.96(3), $b$ = 5.83(3), $c$ = 9.55(1), $\alpha$ = 75.34(2), $\beta$ = 88.92(2), $\gamma$ = 80.64(3) at 2.5 GPa (Figure S7b and Table S1). At ambient conditions, $C_4N_2H_{14}PbCl_4$ is a conventional 1D core−shell quantum wire structure, whose inorganic octahedral chains are surrounded by the organic cations (Figure 3b). At 2.5 GPa, the zigzag rotation of $PbCl_6^{4-}$ octahedra along the $c$-axis accompanied by the unit cell volume collapse appeared (Figures 3c and S8b). The triclinic $C_4N_2H_{14}PbCl_4$ shows an obvious anisotropic compression (Figure S8a). To further clarify the changes inside the crystal structure, we represented the varieties of Pb−Cl bond lengths and Cl−Pb−Cl bond angles upon compression (Figures S9 and S10). When pressure was applied to $C_4N_2H_{14}PbCl_4$, the Pb−Cl−Pb band angle in the *bc* plane obviously decreased from 175.28°(2) at ambient conditions to 160.69°(3) at 2.5 GPa (Figure 3d and e) accompanied by no obvious changes in the Pb−Cl band length (Figure S9), which identified the serious distortion of the interoctahedral chains. Accordingly, such evolution of the inorganic structure triggers the structure phase transition, which is coincident with the new PL emission emergence and the sudden band gap blue-shift. With further compression, the interoctahedron became more distorted as the Pb−Cl−Pb bond angle continuous decrease (Figure S10). Meanwhile, the Pb−Cl bond lengths are defined as $L_1$ and $L_2$ also slowly decreased showing the onset distortion of intraoctahedral structures. When the pressure reached 14.7 GPa, the intraoctahedron shrank severely, which triggers the distinct contraction rate of the $L_1$ bond length and $L_2$ bond length (Figures S9 and S11). This is consistent with the PL intensity re-enhancement in the high pressure range. To further study the evolution of the inorganic sublattice layer, we also carried out high-pressure Raman experiments (Figure S12). The Raman spectra confirmed the structural phase transition at 2.3 GPa and the serious structural distortion above 14.6 GPa.

Analysis of combined *in situ* high-pressure PL, absorption, and time-resolved PL decay dynamics data indicates that the pressure-induced variation of the fascinating optical properties in the $C_4N_2H_{14}PbCl_4$ perovskite crystal is possibly ascribed to the multiple radiative self-trapped states transformation.[17,49]

The mechanism of pressure-induced emission in $C_4N_2H_{14}PbCl_4$ is illustrated in Figure 4a−c. Upon excitation, electrons from the ground state (GS) move into the higher energy free exciton (FE) state and form excited carriers. Although there is an essential difference between the FE state and the free-carrier (FC) state, the changes of the band gaps still contribute to the change of the FE state energy.[50,51] The carriers overcome the activation barrier $E_{trap}$ by thermal activation to realize the transition from the FE states to the multiple STE states or overcome $E_{detrapn}$ ($n$ = 1,2,3) to bring the carriers on the multiple STE states back to the FE states. Multiple STE states located at various energy states led to STE emission with different wavelengths. When an equilibrium is reached between adjacent STE states, a broad band spectrum is achieved. Under ambient conditions, due to the strong quantum confinement in the initial structure, the excited carriers are easily confined to the conduction band to form bound excitons. The bound excitons can relax to the multiple STE states via the route of the downward dark red arrows (Figure 4a). However, partly bound excitons are easily detrapped from the first STE state back to the FE states (shown by the upward dark red arrow in Figure 4a) due to the much smaller detrap energy barrier $E_{detrap1}$ of phase I.[17] Therefore, only the self-trapped states with larger $E_{detrap}$ give emissions in the range around 550 nm (Figure 4a). After 2.0 GPa, the phase transition triggered a sudden increase in the band gap (Figure S6) and the FE state moved to higher position, accompanied by the increase of the $E_{detrap1}$ caused the excited carriers in the first STEs no longer detrapped back to the FE state (Figure 3b).[52−55] Consequently, a new emission peak emerged located around 390 nm. After that, the marked distorted structure highly increased the electron−phonon coupling and the $STE_1$ state became much lower accompanied by a larger $E_{detrap}$ activation energy.[56] Thus, the emission band in the range 390−420 showed dominating emissions and both


https://dx.doi.org/10.1021/jacsau.1c00024
JACS Au 2021, 1, 459−466

emission peaks increase in intensity from 2.0 to 10.5 GPa (Figure S14a). Upon further investigations of PL decay curves at 10.0 GPa, the significantly similar lifetimes of both peaks indicate that both peaks originate from the STE emission (Figure S13a).[17] When the $STE_1$ state reaches the deepest place, $STE_2$ and $STE_3$ began to shift to lower positions and there is competition among STE states. Meanwhile, $E_{trap}$ and $E_{detrap}$ showed a large enhancement, which promotes the nonradiative recombination of STE excitons via the phonon modes of the huge organic cations (Figure S12b).[57] Therefore, although the first emission peak is still at the dominant position, the intensities of both PL peaks decrease continuously with the increase in pressure of 10.5−15.0 GPa. Upon further compression, the position of the STE states will present a reversal where the $STE_2$ and $STE_3$ states become much lower than the $STE_1$ state, which triggers more carriers to be trapped by the $STE_2$ and $STE_3$ states (Figure 4c). Due to the wavelength dependence of STE emission, the decay times can effectively reflect STE state depths; the reversal can be confirmed as shown in Figure S13b. Meanwhile, the obvious intraoctahedral structural distortions not only trigger the distinct band gap decrease and the FE state and $E_{trap}$ decrease but also cause a substantial increase in the electron−phonon coupling, resulting in the STE radiative recombination experiencing a great increase (Figures S9 and S11).[58] Therefore, the emission band at around 550 nm gives dominating emissions and the intensity of both emission peaks increases from 15.0 to 35.1 GPa.

## CONCLUSION

In conclusion, we have demonstrated an unusual pressure-driven optical response and phase transition in 1D halide perovskite $C_4N_2H_{14}PbCl_4$. The results show that PL colors of the broadband STE emission can be easily adjusted between "cold" white light and "warm" white light accompanied by higher CRI. In particular, $C_4N_2H_{14}PbCl_4$ shows a never acquired remarkable PIE phenomenon in the high-pressure area (15.0−35.1 GPa). *In situ* high-pressure ADXRD and the time-resolved PL decay dynamics data show that the distortions of inorganic octahedral chains and the $[PbCl_6]^{4-}$ intraoctahedral unit effectively influence the FE state and STE state position and electron−phonon coupling, which caused the tunable emission chromaticity and STE emission enhancement. This work not only breaks the conventional thinking that the PIE phenomenon only appears in low pressure areas but also provides greater possibility for synthesizing perovskite materials ideal for practical lighting applications.

## ASSOCIATED CONTENT

### Supporting Information

The Supporting Information is available free of charge at https://pubs.acs.org/doi/10.1021/jacsau.1c00024.

Details of the sample preparation and some experiment details; CCTs at selected pressures; absorption and emission spectra; PL spectra; high-pressure UV/vis absorption spectra; Rietveld refinement and cell parameters; lattice constants and experimental volumes; octahedral chain view of $C_4N_2H_{14}PbC_{l4}$; calculated pressure-driven bridging Pb−Cl−Pb angle and Pb−Cl bond length evolution; selected Raman spectra; (PDF)

## AUTHOR INFORMATION


### Corresponding Authors

**Kai Wang** − *State Key Laboratory of Superhard Materials, College of Physics, Jilin University, Changchun 130012, China;* orcid.org/0000-0003-4721-6717; Email: kaiwang@jlu.edu.cn

**Bo Zou** − *State Key Laboratory of Superhard Materials, College of Physics, Jilin University, Changchun 130012, China;* orcid.org/0000-0002-3215-1255; Email: zoubo@jlu.edu.cn

### Authors

**Yuanyuan Fang** − *State Key Laboratory of Superhard Materials, College of Physics, Jilin University, Changchun 130012, China*

**Tianyin Shao** − *State Key Laboratory of Superhard Materials, College of Physics, Jilin University, Changchun 130012, China*

**Long Zhang** − *State Key Laboratory of Superhard Materials, College of Physics, Jilin University, Changchun 130012, China*

**Laizhi Sui** − *State Key Laboratory of Molecular Reaction Dynamics, Dalian Institute of Chemical Physics, Chinese Academy of Sciences, Dalian 116023, China;* orcid.org/0000-0003-3459-9755

**Guorong Wu** − *State Key Laboratory of Molecular Reaction Dynamics, Dalian Institute of Chemical Physics, Chinese Academy of Sciences, Dalian 116023, China;* orcid.org/0000-0002-0212-183X

**Kaijun Yuan** − *State Key Laboratory of Molecular Reaction Dynamics, Dalian Institute of Chemical Physics, Chinese Academy of Sciences, Dalian 116023, China;* orcid.org/0000-0002-5108-8984

Complete contact information is available at: https://pubs.acs.org/10.1021/jacsau.1c00024


### Author Contributions

We thank L.S., G.W. and K.Y. for assistance with the time-resolved PL decay dynamics measurements. Y.F., T.S., and L.Z. performed high pressure optical and XRD experiments. L.S., G.W., and K.Y. carried out the time-resolved PL decay dynamics measurements. Y.F., K.W., and B.Z. wrote the manuscript. All authors discussed and commented on the manuscript.

### Funding

This work is supported by the National Science Foundation of China (NSFC) (Nos. 21725304,11774120). The Graduate Innovation Fund of Jilin University. The Chemical Dynamics Research Center (Grant No. 21688102), the Key Technology Team of the Chinese Academy of Sciences (Grant No. GJJSTD20190002). Angle-dispersive XRD measurement was performed at the 4W2 HP-Station, BSRF.

### Notes

The authors declare no competing financial interest.

## REFERENCES

(1) Gao, P.; Bin, M. Y. A. R.; Nazeeruddin, M. K. Dimensionality engineering of hybrid halide perovskite light absorbers. *Nat. Commun.* **2018**, *9* (1), 5028.

(2) Misra, R. K.; Cohen, B.-E.; Iagher, L.; Etgar, L. Low-Dimensional Organic-Inorganic Halide Perovskite: Structure, Properties, and Applications. *ChemSusChem* **2017**, *10*, 3712−3721.

(3) Lin, H.; Zhou, C.; Tian, Y.; Siegrist, T.; Ma, B. Low-Dimensional Organometal Halide Perovskites. *ACS Energy Lett.* **2018**, *3* (1), 54−62.

(4) Saidaminov, M. I.; Mohammed, O. F.; Bakr, O. M. Low-Dimensional-Networked Metal Halide Perovskites: The Next Big Thing. *ACS Energy Lett.* **2017**, *2* (4), 889−896.
(5) Yusoff, A. R. b. M.; Nazeeruddin, M. K. Low-Dimensional Perovskites: From Synthesis to Stability in Perovskite Solar Cells. *Adv. Energy Mater.* **2018**, *8* (26), 1702073.
(6) Haris, M. P. U.; Bakthavatsalam, R.; Shaikh, S.; Kore, B. P.; Moghe, D.; Gonnade, R. G.; Sarma, D. D.; Kabra, D.; Kundu, J. Synthetic Control on Structure/Dimensionality and Photophysical Properties of Low Dimensional Organic Lead Bromide Perovskite. *Inorg. Chem.* **2018**, *57* (21), 13443−13452.
(7) Liao, Y.; Liu, H.; Zhou, W.; Yang, D.; Shang, Y.; Shi, Z.; Li, B.; Jiang, X.; Zhang, L.; Quan, L. N.; Quintero-Bermudez, R.; Sutherland, B. R.; Mi, Q.; Sargent, E. H.; Ning, Z. Highly Oriented Low-Dimensional Tin Halide Perovskites with Enhanced Stability and Photovoltaic Performance. *J. Am. Chem. Soc.* **2017**, *139* (19), 6693−6699.
(8) Kamminga, M. E.; Fang, H.-H.; Filip, M. R.; Giustino, F.; Baas, J.; Blake, G. R.; Loi, M. A.; Palstra, T. T. M. Confinement Effects in Low-Dimensional Lead Iodide Perovskite Hybrids. *Chem. Mater.* **2016**, *28* (13), 4554−4562.
(9) Zhou, C.; Tian, Y.; Wang, M.; Rose, A.; Besara, T.; Doyle, N. K.; Yuan, Z.; Wang, J. C.; Clark, R.; Hu, Y.; Siegrist, T.; Lin, S.; Ma, B. Low-Dimensional Organic Tin Bromide Perovskites and Their Photoinduced Structural Transformation. *Angew. Chem., Int. Ed.* **2017**, *56* (31), 9018−9022.
(10) Proppe, A. H.; Quintero-Bermudez, R.; Tan, H.; Voznyy, O.; Kelley, S. O.; Sargent, E. H. Synthetic Control over Quantum Well Width Distribution and Carrier Migration in Low-Dimensional Perovskite Photovoltaics. *J. Am. Chem. Soc.* **2018**, *140* (8), 2890−2896.
(11) Grancini, G.; Nazeeruddin, M. K. Dimensional tailoring of hybrid perovskites for photovoltaics. *Nat. Rev. Mater.* **2019**, *4* (1), 4−22.
(12) Wang, S.; Yao, Y.; Wu, Z.; Peng, Y.; Li, L.; Luo, J. Realization of "Warm" White Light Via Halide Substitution in Polar Two-Dimensional Hybrid Perovskites $(2meptH_2)PbCl_xBr_{4-x}$. *J. Mater. Chem. C* **2018**, *6* (45), 12267−12272.
(13) Zhou, N.; Shen, Y.; Li, L.; Tan, S.; Liu, N.; Zheng, G.; Chen, Q.; Zhou, H. Exploration of Crystallization Kinetics in Quasi Two-Dimensional Perovskite and High-Performance Solar Cells. *J. Am. Chem. Soc.* **2018**, *140* (1), 459−465.
(14) Li, L.; Sun, Z.; Wang, P.; Hu, W.; Wang, S.; Ji, C.; Hong, M.; Luo, J. Tailored Engineering of an Unusual $(C_4H_9NH_3)_2(CH_3NH_3)_2Pb_3Br_{10}$ Two-Dimensional Multilayered Perovskite Ferroelectric for a High-Performance Photodetector. *Angew. Chem., Int. Ed.* **2017**, *56* (40), 12150−12154.
(15) Wang, Y.; Song, L.; Chen, Y.; Huang, W. Emerging New-Generation Photodetectors Based on Low-Dimensional Halide Perovskites. *ACS Photonics* **2020**, *7* (1), 10−28.
(16) Yang, R.; Li, R.; Cao, Y.; Wei, Y.; Miao, Y.; Tan, W. L.; Jiao, X.; Chen, H.; Zhang, L.; Chen, Q.; Zhang, H.; Zou, W.; Wang, Y.; Yang, M.; Yi, C.; Wang, N.; Gao, F.; McNeill, C. R.; Qin, T.; Wang, J.; Huang, W. Oriented Quasi-2D Perovskites for High Performance Optoelectronic Devices. *Adv. Mater.* **2018**, *30*, 1804771.
(17) Wu, G.; Zhou, C.; Ming, W.; Han, D.; Chen, S.; Yang, D.; Besara, T.; Neu, J.; Siegrist, T.; Du, M.-H.; Ma, B.; Dong, A. A One-Dimensional Organic Lead Chloride Hybrid with Excitation-Dependent Broadband Emissions. *ACS Energy Lett.* **2018**, *3* (6), 1443−1449.
(18) Liu, G.; Gong, J.; Kong, L.; Schaller, R. D.; Hu, Q.; Liu, Z.; Yan, S.; Yang, W.; Stoumpos, C. C.; Kanatzidis, M. G.; Mao, H.-k.; Xu, T. Isothermal Pressure-Derived Metastable States in 2D Hybrid Perovskites Showing Enduring Bandgap Narrowing. *Proc. Natl. Acad. Sci. U. S. A.* **2018**, *115* (32), 8076−8081.
(19) Ji, C.; Li, B.; Liu, W.; Smith, J. S.; Majumdar, A.; Luo, W.; Ahuja, R.; Shu, J.; Wang, J.; Sinogeikin, S.; Meng, Y.; Prakapenka, V. B.; Greenberg, E.; Xu, R.; Huang, X.; Yang, W.; Shen, G.; Mao, W. L.; Mao, H. K. Ultrahigh-Pressure Isostructural Electronic Transitions in Hydrogen. *Nature* **2019**, *573* (7775), 558−562.
(20) Yin, T.; Liu, B.; Yan, J.; Fang, Y.; Chen, M.; Chong, W. K.; Jiang, S.; Kuo, J. L.; Fang, J.; Liang, P.; Wei, S.; Loh, K. P.; Sum, T. C.; White, T. J.; Shen, Z. X. Pressure-Engineered Structural and Optical Properties of Two-Dimensional $(C_4H_9NH_3)_2PbI_4$ Perovskite Exfoliated nm-Thin Flakes. *J. Am. Chem. Soc.* **2019**, *141* (3), 1235−1241.
(21) Jaffe, A.; Lin, Y.; Mao, W. L.; Karunadasa, H. I. Pressure-Induced Conductivity and Yellow-to-Black Piezochromism in a Layered Cu-Cl Hybrid Perovskite. *J. Am. Chem. Soc.* **2015**, *137* (4), 1673−1678.
(22) Ma, Z.; Li, F.; Zhao, D.; Xiao, G.; Zou, B. Whether or Not Emission of $Cs_4PbBr_6$ Nanocrystals: High-Pressure Experimental Evidence. *CCS Chem.* **2020**, *2* (2), 71−80.
(23) Huang, Z.; Auckett, J. E.; Blanchard, P. E.; Kennedy, B. J.; Miiller, W.; Zhou, Q.; Avdeev, M.; Johnson, M. R.; Zbiri, M.; Garbarino, G.; Marshall, W. G.; Gu, Q.; Ling, C. D. Pressure-Induced Intersite Bi-M (M = Ru, Ir) Valence Transitions in Hexagonal Perovskites. *Angew. Chem., Int. Ed.* **2014**, *53* (13), 3414−3417.
(24) Bai, F.; Bian, K.; Huang, X.; Wang, Z.; Fan, H. Pressure Induced Nanoparticle Phase Behavior, Property, and Applications. *Chem. Rev.* **2019**, *119* (12), 7673−7717.
(25) Wang, L.; Wang, K.; Xiao, G.; Zeng, Q.; Zou, B. Pressure-Induced Structural Evolution and Band Gap Shifts of Organometal Halide Perovskite-Based Methylammonium Lead Chloride. *J. Phys. Chem. Lett.* **2016**, *7* (24), 5273−5279.
(26) Nguyen, L. A. T.; Minh, D. N.; Yuan, Y.; Samanta, S.; Wang, L.; Zhang, D.; Hirao, N.; Kim, J.; Kang, Y. Pressure-Induced Fluorescence Enhancement of $FA_\alpha PbBr_{2+\alpha}$ Composite Perovskites. *Nanoscale* **2019**, *11* (13), 5868−5873.
(27) Wang, Y.; Lu, X.; Yang, W.; Wen, T.; Yang, L.; Ren, X.; Wang, L.; Lin, Z.; Zhao, Y. Pressure-Induced Phase Transformation, Reversible Amorphization, and Anomalous Visible Light Response in Organolead Bromide Perovskite. *J. Am. Chem. Soc.* **2015**, *137* (34), 11144−11149.
(28) Liu, S.; Sun, S.; Gan, C. K.; Aguila, A. G. D.; Fang, Y.; Xing, J.; Do, T. T. H.; White, T. J.; Li, H.; Huang, W.; Xiong, Q. Manipulating Efficient Light Emission in Two-Dimensional Perovskite Crystals by Pressure-Induced Anisotropic Deformation. *Sci. Adv.* **2019**, *5*, No. eaav9445.
(29) Yuan, Y.; Liu, X. F.; Ma, X.; Wang, X.; Li, X.; Xiao, J.; Li, X.; Zhang, H. L.; Wang, L. Large Band Gap Narrowing and Prolonged Carrier Lifetime of $(C_4H_9NH_3)_2PbI_4$ under High Pressure. *Adv. Sci.* **2019**, *6* (15), 1900240.
(30) Chen, Y.; Fu, R.; Wang, L.; Ma, Z.; Xiao, G.; Wang, K.; Zou, B. Emission Enhancement and Bandgap Retention of a Two-Dimensional Mixed Cation Lead Halide Perovskite Under High Pressure. *J. Mater. Chem. A* **2019**, *7* (11), 6357−6362.
(31) Zhang, L.; Liu, C.; Wang, L.; Liu, C.; Wang, K.; Zou, B. Pressure-Induced Emission Enhancement, Band-Gap Narrowing, and Metallization of Halide Perovskite $Cs_3Bi_2I_9$. *Angew. Chem., Int. Ed.* **2018**, *57* (35), 11213−11217.
(32) Fang, Y.; Zhang, L.; Wu, L.; Yan, J.; Lin, Y.; Wang, K.; Mao, W. L.; Zou, B. Pressure-Induced Emission (PIE) and Phase Transition of a Two-dimensional Halide Double Perovskite $(BA)_4AgBiBr_8$ (BA = $CH_3(CH_2)_3NH_3^+$). *Angew. Chem., Int. Ed.* **2019**, *58*, 15249−15253.
(33) Qin, Y.; Lv, Z.; Chen, S.; Li, W.; Wu, X.; Ye, L.; Li, N.; Lu, P. Tuning Pressure-Induced Phase Transitions, Amorphization, and Excitonic Emissions of 2D Hybrid Perovskites via Varying Organic Amine Cations. *J. Phys. Chem. C* **2019**, *123* (36), 22491−22498.
(34) Gao, C.; Li, R.; Li, Y.; Wang, R.; Wang, M.; Gan, Z.; Bai, L.; Liu, Y.; Zhao, K.; Liu, S. F.; Cheng, Y.; Huang, W. Direct-Indirect Transition of Pressurized Two-Dimensional Halide Perovskite: Role of Benzene Ring Stack Ordering. *J. Phys. Chem. Lett.* **2019**, *10* (19), 5687−5693.
(35) Shen, P.; Vogt, T.; Lee, Y. Pressure-Induced Enhancement of Broad-Band White Light Emission in Butylammonium Lead Bromide. *J. Phys. Chem. Lett.* **2020**, *11*, 4131−4137.
(36) Shi, Y.; Ma, Z.; Zhao, D.; Chen, Y.; Cao, Y.; Wang, K.; Xiao, G.; Zou, B. Pressure-Induced Emission (PIE) of One-Dimensional Organic Tin Bromide Perovskites. *J. Am. Chem. Soc.* **2019**, *141* (16), 6504−6508.
(37) Wang, L.; Yao, P.; Wang, F.; Li, S.; Chen, Y.; Xia, T.; Guo, E.; Wang, K.; Zou, B.; Guo, H. Pressure-Induced Structural Evolution and Bandgap Optimization of Lead-Free Halide Double Perovskite $(NH_4)_2SeBr_6$. *Adv. Sci.* **2020**, *7* (6), 1902900.


https://dx.doi.org/10.1021/jacsau.1c00024
*JACS Au* 2021, 1, 459−466

(38) Fang, Y.; Zhang, L.; Yu, Y.; Yang, X.; Wang, K.; Zou, B. Manipulating Emission Enhancement and Piezochromism in Two Dimensional Organic-Inorganic Halide Perovskite $[(HO)(CH_2)_2NH_3)]_2PbI_4$ by High Pressure. *CCS Chem.* DOI: 10.31635/ccschem.020.202000430 (in press).
(39) Liu, G.; Kong, L.; Guo, P.; Stoumpos, C. C.; Hu, Q.; Liu, Z.; Cai, Z.; Gosztola, D. J.; Mao, H. K.; Kanatzidis, M. G.; Schaller, R. D. Two Regimes of Bandgap Red Shift and Partial Ambient Retention in Pressure-Treated Two-Dimensional Perovskites. *ACS Energy Lett.* **2017**, *2*, 2518−2524.
(40) Wang, Y.; Guo, S.; Luo, H.; Zhou, C.; Lin, H.; Ma, X.; Hu, Q.; Du, M. H.; Ma, B.; Yang, W.; Lu, X. Reaching 90% Photoluminescence Quantum Yield in One-Dimensional Metal Halide $C_4N_2H_{14}PbBr_4$ by Pressure-Suppressed Nonradiative Loss. *J. Am. Chem. Soc.* **2020**, *142*, 16001−16006.
(41) Xu, Q.; Stroppa, A.; Lv, J.; Zhao, X.; Yang, D.; Biswas, K.; Zhang, L. Impact of organic molecule rotation on the optoelectronic properties of hybrid halide perovskites. *Phys. Rev. Mater.* **2019**, *3*, 125401.
(42) Tang, Z.; Yao, C.; Zeng, Y.; Huang, Y.; Zhang, L.; Yang, Y.; Sun, C. Anomalous H-C bond thermal contraction of the energetic nitromethane. *J. Mol. Liq.* **2020**, *314*, 113817.
(43) Liu, Z.; Na, G.; Tian, F.; Yu, L.; Li, J.; Zhang, L. Computational functionality-driven design of semiconductors for optoelectronic applications. *Info. Mater.* **2020**, *2*, 879−904.
(44) Zhang, L.; Wu, L.; Wang, K.; Zou, B. Pressure-Induced Broadband Emission of 2D Organic-Inorganic Hybrid Perovskite $(C_6H_5C_2H_4NH_3)_2PbBr_4$. *Adv. Sci.* **2019**, *6* (2), 1801628.
(45) Zhang, L.; Liu, C.; Lin, Y.; Wang, K.; Ke, F.; Liu, C.; Mao, W. L.; Zou, B. Tuning Optical and Electronic Properties in Low-Toxicity Organic-Inorganic Hybrid $(CH_3NH_3)_3Bi_2I_9$ under High Pressure. *J. Phys. Chem. Lett.* **2019**, *10* (8), 1676−1683.
(46) Yin, T.; Fang, Y.; Chong, W. K.; Ming, K. T.; Jiang, S.; Li, X.; Kuo, J. L.; Fang, J.; Sum, T. C.; White, T. J.; Yan, J.; Shen, Z. X. High-Pressure-Induced Comminution and Recrystallization of $CH_3NH_3PbBr_3$ Nanocrystals as Large Thin Nanoplates. *Adv. Mater.* **2018**, *30* (2), 1705017.
(47) Guo, S.; Zhao, Y.; Bu, K.; Fu, Y.; Luo, H.; Chen, M.; Hautzinger, M. P.; Wang, Y.; Jin, S.; Yang, W.; Lu, X. Pressure-Suppressed Carrier Trapping Leads to Enhanced Emission in Two-Dimensional Perovskite $(HA)_2(GA)Pb_2I_7$. *Angew. Chem., Int. Ed.* **2020**, *132*, 2−9.
(48) Ma, Z.; Liu, Z.; Lu, S.; Wang, L.; Feng, X.; Yang, D.; Wang, K.; Xiao, G.; Zhang, L.; Redfern, S. A. T.; Zou, B. Pressure-induced emission of cesium lead halide perovskite nanocrystals. *Nat. Commun.* **2018**, *9* (1), 4506.
(49) Yuan, Z.; Zhou, C.; Tian, Y.; Shu, Y.; Messier, J.; Wang, J. C.; van de Burgt, L. J.; Kountouriotis, K.; Xin, Y.; Holt, E.; Schanze, K.; Clark, R.; Siegrist, T.; Ma, B. One-dimensional organic lead halide perovskites with efficient bluish white-light emission. *Nat. Commun.* **2017**, *8*, 14051.
(50) Zhao, C.; Tian, W.; Sun, Q.; Yin, Z.; Leng, J.; Wang, S.; Liu, J.; Wu, K.; Jin, S. Trap-Enabled Long-Distance Carrier Transport in Perovskite Quantum Wells. *J. Am. Chem. Soc.* **2020**, *142* (35), 15091−15097.
(51) Lian, L.; Zheng, M.; Zhang, P.; Zheng, Z.; Du, K.; Lei, W.; Gao, J.; Niu, G.; Zhang, D.; Zhai, T.; Jin, S.; Tang, J.; Zhang, X.; Zhang, J. Photophysics in $Cs_3Cu_2X_5$ (X = Cl, Br, or I): Highly Luminescent Self-Trapped Excitons from Local Structure Symmetrization. *Chem. Mater.* **2020**, *32* (8), 3462−3468.
(52) Nishimura, H.; Tsujimoto, T.; Nakayama, M.; Morita, S.; Kobayashi, M. Spectral changes of the self-trapped exciton luminescence in RbI under hydrostatic pressure. *J. Lumin.* **1994**, *62*, 41−47.
(53) Tsujimoto, T.; Nishimura, H.; Nakayama, M. Hydrostatic pressure effects on the free and self-trapped exciton states in CsI. *Phys. Rev. B: Condens. Matter Mater. Phys.* **1996**, *54* (23), 16579−16584.
(54) Kurisu, H.; Komatsu, T.; Karasawa, T. Hydrostatic Pressure Effects on the Excitons and Exciton-Phonon in $BiI_3$ Crystals. *J. Phys. Soc. Jpn.* **1993**, *62* (3), 1048−1056.
(55) Gautier, R.; Massuyeau, F.; Galnon, G.; Paris, M. Lead Halide Post-Perovskite-Type Chains for High-Efficiency White-Light Emission. *Adv. Mater.* **2019**, *31* (14), No. e1807383.
(56) Li, Q.; Chen, Z.; Yang, B.; Tan, L.; Xu, B.; Han, J.; Zhao, Y.; Tang, J.; Quan, Z. Pressure-Induced Remarkable Enhancement of Self-Trapped Exciton Emission in One-Dimensional $CsCu_2I_3$ with Tetrahedral Units. *J. Am. Chem. Soc.* **2020**, *142* (4), 1786−1791.
(57) Gautier, R.; Paris, M.; Massuyeau, F. Exciton Self-Trapping in Hybrid Lead Halides: Role of Halogen. *J. Am. Chem. Soc.* **2019**, *141* (32), 12619−12623.
(58) Kawano, N.; Koshimizu, M.; Sun, Y.; Yahaba, N.; Fujimoto, Y.; Yanagida, T.; Asai, K. Effects of Organic Moieties on Luminescence Properties of Organic-Inorganic Layered Perovskite-Type Compounds. *J. Phys. Chem. C* **2014**, *118* (17), 9101−9106.


https://dx.doi.org/10.1021/jacsau.1c00024
*JACS Au* 2021, 1, 459−466